APS physics

CHORUS

This is the accepted manuscript made available via CHORUS. The article has been published as:

Electron Shock Ignition of Inertial Fusion Targets

W. L. Shang, R. Betti, S. X. Hu, K. Woo, L. Hao, C. Ren, A. R. Christopherson, A. Bose, and W. Theobald

Phys. Rev. Lett. **119**, 195001 — Published 7 November 2017

DOI: 10.1103/PhysRevLett.119.195001

Electron shock ignition of inertial fusion targets

W. L. Shang,[1,2] R. Betti,[1,2] S. X. Hu,[3] K. Woo,[1,2] L. Hao,[2] C. Ren,[2,3] A. R. Christopherson,[1,2] A. Bose,[1,2] W. Theobald[1]

[1]Fusion Science Center and Laboratory for Laser Energetics, University of Rochester, Rochester, NY 14623

[2]Departments of Mechanical Engineering and Physics & Astronomy, University of Rochester, Rochester, NY 14623

[3]Laboratory for Laser Energetics, University of Rochester, Rochester, NY 14623

It is shown that inertial confinement fusion (ICF) targets designed with low implosion velocities can be shock-ignited using laser-plasma interaction (LPI) generated hot electrons (hot-e's) to obtain high energy gains. These designs are robust to multimode asymmetries and are predicted to ignite even for significantly distorted implosions. Electron shock ignition requires tens of kilojoules of hot-e's which can only be produced on a large laser facility like the National Ignition Facility (NIF), with the laser-to-hot-e conversion efficiency greater than 10% at laser intensities ~ 10^{16} W/cm^2.

PACS numbers: 52.57.-z, 52.40.Mj, 52.57.Bc, 52.57.Fg

Recent theoretical and experimental results have suggested that launching a spherically convergent shock wave at the end of the acceleration phase improves the

ignition conditions for ICF implosions [1-10]. Such an ICF scheme with a late shock is referred to as "shock ignition". Shock ignition is a scheme that is based on the principles of conventional central hot-spot ignition [11] and uses a late shock to augment the compression of the central hot spot above the ignition threshold. In a shock-ignition implosion, the main pulse used to assemble the dense core is a conventional low-adiabat laser pulse and the target is typically a thick cryogenic shell [1,6,12]. By launching a shock at the end of the main laser pulse, the hot-spot pressure is significantly enhanced and the energy required for ignition decreases by the factor $\Phi \approx \left(P_{\text{shock}}/P_{\text{noshock}}\right)^{2-3}$, where P_{shock} is the hot-spot pressure enhanced by the shock and P_{noshock} is the hot-spot pressure without shock [1]. Because of their large mass, thick shells are driven at low implosion velocities, leading to a significantly lower in-flight aspect ratio (IFAR) and better hydrodynamic stability. Up-to-date, shock-ignition designs use an ignitor shock launched by a spike in the laser power at the end of the pulse. The shock-launching pressure needs to exceed ~ 300 Mbar at laser intensities ~ 10^{16} W/cm^2 [3]. Since the early work on shock ignition [1-10,12], it has been noted that hot-e's are produced at high laser intensities and it has been argued that such electrons can enhance the ignitor shock strength if stopped near the target's outer surface [13]. The ablation pressure resulting from a monoenergetic electron beam stopped on the surface and driving mass ablation has been recently estimated [14-16]. Recent experiments on OMEGA have shown a strong correlation between the shock strength and the hard x-ray signal from hot-e's [3,17]. Radiation–hydrodynamic simulations of these experiments indicate that hot-e's from stimulated Raman scattering (SRS) have increased the shock pressure by hundreds

of Mbars. The overall conversion from laser to hot-e energy was measured to be about 7% with instantaneous values reaching up to 15% at the end of the laser pulse [17].

In this Letter we show that it is possible to design a DT target that can be ignited by hot-e's from LPI using laser energies that are achievable on NIF. A sketch of the concept is shown in Fig. 1(a) illustrating the ignitor shock driven by hot electrons and timed with the rebound shock as in conventional shock ignition [1]. The hot-e source is simulated using a PIC code. Because of the longer plasma scale length, NIF-size targets are expected to exhibit a significantly higher laser-to-hot-e conversion efficiency than OMEGA. Like on OMEGA, hot-e's on the NIF would be produced by SRS. In addition to enhancing the rocket effect [15], hot-e's can also directly augment the static shell pressure thus driving a strong shock. This is a new mechanism of shock launching. The static pressure enhancement occurs when the hot-e mean free path is a finite fraction of the shell thickness. At high temperatures (60 - 70 keV) and for a Maxwellian distribution, the hot-e's do not deposit their energy in a narrow region near the target outer surface causing mass ablation and a rocket effect. Instead, the electrons penetrate into a significant fraction of the target thickness and raise its static pressure without causing mass ablation. The sudden increase in pressure of the outer shell layer drives a strong shock inward with a launching pressure in the gigabar range. Depending on the shell areal density, the hot-e energy and angular spread, the hot-e drive could be more effective than the laser-driven ablation pressure, and produce stronger ignitor shocks and final hot spot pressures. In this case, even very low velocity (V_{imp} ~ 200 km/s) targets can be ignited. In this paper, we denote this implosion scheme with a hot-e driven shock as "electron shock ignition".

To make the physics case for electron shock ignition, we first compare the effects on the hot spot pressure of hot-e versus laser driven shocks using the simple planar shock-ignition model of Ref. [18] [shown in Fig. 1(b)]. In this model, a lower density plasma (the hot spot) is compressed by a planar compressible piston with a given initial velocity. The piston is shocked by an external pulse of either direct laser illumination or hot electrons. ~~The results are validated by lagrangian hydrodynamic simulations.~~ The model calculates the trajectories and properties of shocks propagating through the high density foil and low density gas (hot spot). We assume that all of the LPIs have taken place and we are left with a compressible piston driven by an applied pressure. In pure hydrodynamics, the major indicator of target performance is the final hot spot pressure.

The planar model uses initial conditions (density, pressure, temperature, and velocity) from a one-dimensional *LILAC* [19] simulation of a target similar to the proposed NIF shock-ignition target design in Ref. [20]. The target, shown in Fig. 2 has a 1080-μm-outer-radius, 161-μm-thick DT ice layer, and 31-μm-thick plastic ablator [Fig. 2(a)]. The target is driven by the UV-laser pulse in Fig. 2(b). The pulse shape [solid curve in Fig. 2(b)] consists of an adiabat-shaping [21] 310 kJ fuel-assembly pulse with two pickets setting the DT ice on an inner adiabat $\alpha \sim 1.8$, and driving shell to a low implosion velocity of $V_{\text{imp}} \sim 200$ km/s. The fuel-assembly pulse is followed by a 200 ps, 100 kJ power spike with intensity 3.4×10^{15} W/cm^2 to launch the ignitor shock. The shock launching mechanism is either conventional laser ablation or hot-e energy deposition. The laser ablation pressure is approximated by [22]:

$$P_{\mathrm{Mbar}} = 40\left(\frac{I_{15}^{\mathrm{L}}}{\lambda_{\mu\mathrm{m}}}\right)^{2/3}, \tag{1}$$

where I_{15}^{L} is the laser intensity in 10^{15} W/cm^2 and $\lambda_{\mu\mathrm{m}}$ is the laser wavelength in μm. For the hot-e drive, the shock formation in a dense plasma by an intense electron beam can occur in two ways. If the hot-e stopping length is much shorter than the target thickness, then the hot-e heating causes mass ablation and the ignitor shock is driven by the rocket effect. This is the case described in Ref. [15], where the hot-e induced ablation pressure follows the rocket-effect formula:

$$P_{\mathrm{Gbar}} = 0.6\left(\frac{\eta}{0.2}\right)^{2/3}\left(\frac{I_{15}^{\mathrm{L}}}{10}\right)^{2/3}\left(\frac{\rho_{\mathrm{g/cm^3}}}{10}\right)^{1/3}, \tag{2}$$

where $\rho_{\mathrm{g/cm^3}}$ is the mass density in g/cm^3 and η is the conversion efficiency of laser energy to hot-e energy. For a fixed η, the hot-e induced ablation pressure exceeds the laser-induced ablation pressure at higher densities. If the electron stopping length is a finite fraction of the in-flight shell thickness, then the ignitor shock is launched by direct heating of the target. This is likely the most relevant case for electron shock ignition and is first described here. In this case, the shock-launching pressure can be estimated in the limit of a hot-e deposition time shorter than the hydroydynamic time, leading to $P \approx (2/3)E_{\mathrm{h}}/V_{\mathrm{h}}$, where V_{h} is the shell volume heated by the hot-e's and E_{h} is the deposited hot-e energy. We use the hot-e stopping range averaged over a Maxwellian

distribution with temperature T_h. $\rho_{g/cm^3} R_{cm} \approx 0.015\left(\frac{T_h^{keV}}{60}\right)^{1.6}$, which is valid for the energy range $10 < T_h^{keV} < 400$ of interest to shock ignition. A similar scaling law $T_h^{1.67}$ was derived in Ref. [23]. Using the above stopping range, the shock-launching pressure can be approximated by

$$P_{\mathrm{Gbar}} \approx 1.33\left(\frac{I_{15}^{\mathrm{L}}}{10}\right)\left(\frac{\rho_{\mathrm{g/cm^3}}}{10}\right)\left(\frac{60}{T_{\mathrm{h}}^{\mathrm{keV}}}\right)^{1.6}\left(\frac{\eta}{0.2}\right)\left(\frac{\tau_{ns}}{0.2}\right), \quad (3)$$

where τ_{ns} is the ignitor spike duration in ns. The derivation of Eq. (3) originates from the ratio of the hot electron energy flux and the stopping length similarly to the analysis in Ref. [24]. Note that in the low T_{h} limit (short propagation range), Eq. (3) is not valid and one should instead use Eq. (2).

The laser ignitor spike is shown in Fig. 2(b) with different values of η as 10%, 15%, and 20%. Recent experiments on OMEGA indicate that up to 15% of the instantaneous laser energy is converted into hot-e's in plastic ablators when smoothing by spectral dispersion (SSD) is turned off [17]. Full-aperture backscatter station (FABS) spectra show that SRS is the dominant hot-e production process. Simulations of SRS-driven hot-e's were performed using the PIC code OSIRIS [25,26]. The simulated density region extended from 0.2 to 0.3 n_c (n_c is the critical density), to capture the SRS absolute instability that is the main drive for hot-e generation. It is reported that in shock ignition plasma, SRS can take place only in the vicinity of the quarter critical density [27], and the

simulation region in Ref. [26] is set from 0.17 to 0.33 n_c. The 1D PIC simulation parameters are taken from LILAC simulations of the target design in Fig. 2 during the laser spike, with T_e = 8 keV, T_i = 1.5 keV, and the plasma scale length about 314 μm. In Fig. 3(a), the laser-to-hot-e conversion efficiency is $\eta_{50} \sim 25\%$ for hot-e energy above 50 keV, and is $\eta_{25} \sim 31\%$ for energy above 25 keV. Previous PIC simulations with a shorter OMEGA-shock-ignition plasma scale length of 170 μm shows $\eta_{50} \sim 19\%$ in agreement with experimental results [26].

In the planar model [Fig. 1(b)], the maximum hot spot pressure is used to compare the effects of laser driven [Eq. (1)] to hot-e driven shocks [Eq. (2) and (3)]. The ratio of hot spot pressures is denoted as $R = P_{\text{hot-e}} / P_{\text{laser}}$. Figure 3(b) shows that the ratio R is dependent on the shock-driven scheme and the laser-to-hot-e conversion efficiency η. For the rocket-effect hot-e deposition scheme [Eq. (2)], $R > 1$ when η is over 10% and the hot-e's can generate higher hot spot pressures than laser ablation. If 20% of the laser energy is converted to hot-e's, R increases to 1.3. Since $\eta \sim 15\%$ is measured/computed on OMEGA [17, 26], and a larger $\eta \sim 25\%$ is obtained in PIC simulations of NIF-scale targets, sufficient hot-e energy can be provided for electron shock ignition on NIF. For the static pressure hot-e-deposition scheme [Eq. (3)], $\eta \sim 15\%$ leads to R of 1.8, and R = 2.8 can be achieved when η increases to 20%, indicating large hot spot pressure enhancements. It should be noted that in Fig. 3(b), the pressure enhancement windows for various η are similar to the ignition windows for shock ignition [28]. The ignition window varies with the hot-e energy deposition scheme and the laser to hot-e conversion efficiency η.

The simple planar model above provides a simple estimate of the beneficial effects of hot-e driven shocks. For a detailed evaluation of electron shock ignition, we simulated hot-e driven shocks using the two-dimensional eulerian radiation hydrodynamics code *DEC2D* [29-31] including a two-fluid description, thermal and radiation transport, and alpha diffusion. *DEC2D* uses a moving mesh scheme that maintains a high resolution throughout the final convergence. The hot-e deposition is included to *DEC2D* using the stopping power model of Ref. [32]. Binary collisions and exciting plasma waves effects are the mechanisms for the slowing down of hot-e's. Lewis's multiple scattering theory [33] is used to calculate the spatial moments of the electron-distribution function. A Maxwellian electron beam with T_e = 60 keV (as from PIC simulations in Fig. 3(a) and the OMEGA experiments [17,34]) is injected in the compressed moving shell in the calculation, and 50-group hot-e energy distribution up to 400 keV is used. The radial profiles of density, pressure, velocity, and temperature from *LILAC* simulations of the target in Fig. 2 at the end of the assembly pulse are used as initial conditions for *DEC2D*. The hot-e's are injected during the power spike. The hot-e generated pressure is shown in Fig. 4(a) and compared with the pressure without hot-e's. A peak pressure of 2 Gbar [Fig. 4(a)] is achieved with hot-e energy of 25 kJ and launching time of 10.3 ns. The mean pressure over the deposition region is about half its peak value which is in general agreement with ~ 0.7 Gbar from Eq.(3).

In shock ignition, if the ignitor shock is launched too early in time, the incoming strong shock will go through the inner shell surface, and collide with the outgoing rebound shock in the low density hot spot. In this case there will not be a secondary shell piston effect, which is the main characteristic of shock ignition requiring the collision

between the incoming and outgoing shocks to occur inside the shell near the inner shell surface [1]. An early shock leads to low hot spot pressures, preventing ignition to occur. Conversely, if the ignitor shock is launched too late, it will collide with the outgoing rebound shock near the shell outer surface. In this case, the collision occurs too late (near or past the stagnation time) and it does not improve the ignition conditions. Thus, shock ignition exhibits an ignition window for the ignitor shock launching time [28]. Figure 4(b) shows the ignition windows for electron shock ignition calculated by *DEC2D* for a uniform implosion (1D). The target ignites when the hot-e energy exceeds 10 kJ. The gain increases with the hot-e energy, and gain ~ 130 is achieved with a hot-e energy of 40 kJ. For a laser-to-hot-e conversion efficiency of η ~ 15%, a 500 TW laser pulse with duration of 200 ps can generate 15 kJ hot-e's. The hot-e energy goes up to 20 kJ with η ~ 20%, leading to gain ~ 100 with this target. In addition, the ignition window broadens as the hot-e energy increases, indicating that more energy makes the implosion less sensitive to ignitor shock mistiming. It is important to emphasize that electron shock ignition requires targets with enough areal densities to stop the hot-e's and prevent preheat of the inner shell layer. As shown in Ref. [35,36], preheat of the inner portion of the shell leads to low hot spot pressure thereby preventing ignition to occur.

The hydrodynamic code *DEC2D* was used extensively to investigate the effects of nonuniformities on the deceleration phase of ICF implosions [29-31]. Here *DEC2D* is used to study the effect of nonuniformities on the hot-e driven shock ignition by varying the nonuniformity spectrum applied on the target. Nonuniformities are included as density perturbations at the end of the fuel assembly pulse. Different nonuniformity spectra are considered. Multimode roughness of NIF direct drive capsule spectrum from

mode 2 to 60 [37], multimode roughness of OMEGA direct drive capsule spectrum from mode 2 to 300 [38], and single-mode 10 simulations with various initial density perturbation amplitudes from 1% to 10% were carried out (mode 10 is the dominant illumination nonuniformity due to the port geometry on OMEGA). Remarkably, the performance degradation can be expressed in a way independent of the nonuniformity spectrum. This is done through the metric used in Ref. [39], to measure the level of nonuniformities, the yield over clean (1D) in the absence of α-particle deposition $\mathrm{YOC}_{\mathrm{no}\alpha}$. This parameter represents the degradation in yield due to the effect of nonuniformities on the pure hydrodynamic performance.

The level of nonuniformity is increased until ignition fails. $\mathrm{YOC}_{\mathrm{no}\alpha}$ is determined by repeating each run without the α-particle energy deposition to obtain the noα neutron yield. A gain curve is generated by plotting the energy gain (fusion energy yield/laser energy on target) versus $\mathrm{YOC}_{\mathrm{no}\alpha}$. Figure 5(a) shows the gain curves for 25 kJ hot-e driven shock ignition with the target in Fig. 2. Two times are selected: at 10.3 ns in the middle of the ignition window in Fig. 4(b), and 10.5 ns near the ignition cliff. As shown in Fig. 5(a), a launching time of 10.3 ns leads to a more robust performance with ignition occuring for large nonuniformities down to $\mathrm{YOC}_{\mathrm{no}\alpha} \sim 0.5$. A shock launched at 10.5 ns ignites the target for a nonuniformity level as low as $\mathrm{YOC}_{\mathrm{no}\alpha} \sim 0.8$. This implies that the capsule in the cener of the ignition window is more robust than that near the ignition cliff. The density plots at the peak neutron rate for a low gain ~ 4 at 10.3 ns with and without α-heating are shown in Fig. 5(b) and 5(c).

It is shown in Ref. [40] that the yield amplification due to α-heating ($\hat{Y}_{\text{amp}} = Y_{\alpha}/Y_{no\alpha}$) depends almost exclusively on the generalized Lawson parameter $\chi_{\text{no}\alpha}$. Since $\chi_{no\alpha} \sim YOC_{no\alpha}^{0.4}$, we expect to see similar degration in yields from different sources of nonuniformities as long as $\text{YOC}_{\text{no}\alpha}$ is the same. Indeed, Fig. 5(a) shows that the fusion gain depends exclusively on $\text{YOC}_{\text{no}\alpha}$, and is independent on the nonuniformity spectrum and amplitude.

In summary, electron shock ignition is a plausible path to ignition and high gains for inertial fusion. Hot-e's are used to launch the ignitor shock. Ignition occurs for the hot-e energies of tens of kilojoules. For the target of Ref. [20], the minimum hot-e energy required for ignition is about 10 kJ with the laser-to-hot-e conversion efficiency $\eta \sim 10\%$. As indicated by recent OMEGA experiments and PIC simulations of absolute SRS, values of 20% may be achievable with MJ-scale lasers. High gains of ~ 100 can be achieved when $\eta > 20\%$. Hot-e driven shock ignition is robust to multimode asymmetries and ignition can be achieved for $\text{YOC}_{\text{no}\alpha}$ as low as 0.5.

Acknowledgment and Disclaimer

This work has been supported by the U.S. Department of Energy under Cooperative Agreements DE-FC02-04ER54789 (Office of Fusion Energy Sciences), DE-NA0001944 (National Nuclear Security Administration) by the NYSERDA, DE-SC0012316 (Office of Fusion Energy Sciences), and Grant NO. YZJJLX 2016007 by the Presidential Foundation of CAEP.

References

1. R. Betti, C. D. Zhou, K. S. Anderson, L. J. Perkins, W. Theobald, and A. A. Solodov, Phys. Rev. Lett. **98**, 155001 (2007).
2. S. Atzeni, A. Marocchino, A. Schiavi, and G. Schurtz, New J. Phys. **15**, 045004 (2013).
3. R. Nora, W. Theobald, R. Betti, F. J. Marshall, D. T. Michel, W. Seka, B. Yaakobi, M. Lafon, C. Stoeckl, J. A. Delettrez *et al.*, Phys. Rev. Lett. **114**, 045001 (2015).
4. S. Atzeni, X. Ribeyre, G. Schurtz, A. J. Schmitt, B. Canaud, R. Betti, and L. J. Perkins, Nucl. Fusion **54**, 054008 (2014).
5. D. Batani, S. Baton, A. Casner, S. Depierreux, M. Hohenberger, O. Klimo, M. Koenig, C. Labaune, X. Ribeyre, C. Rousseaux *et al.*, Nucl. Fusion **54**, 054009 (2014).
6. L. J. Perkins, R. Betti, K. N. LaFortune, and W. H. Williams, Phys. Rev. Lett. **103**, 045004 (2009).
7. W. Theobald, R. Betti, C. Stoeckl, K. S. Anderson, J. A. Delettrez, V. Yu. Glebov, V. N. Goncharov, F. J. Marshall, D. N. Maywar, R. L. McCrory *et al.*, Phys. Plasmas **15**, 056306 (2008).
8. M. Lafon, X. Ribeyre, and G. Schurtz, Phys. Plasmas **20**, 022708 (2013).
9. A. J. Schmitt, J. W. Bates, S. P. Obenschain, S. T. Zalesak, and D. E. Fyfe, Phys. Plasmas **17**, 042701 (2010).
10. X. Ribeyre, V. T. Tikhonchuk, J. Breil, M. Lafon, and E. Le Bel, Phys. Plasmas **18**, 102702 (2011).

11. S. Atzeni and J. Meyer-ter-vehn, The Physics of Inertial Fusion (Clarendon, Oxford, 2004).

12. B. Canaud and M. Temporal, New J. Phys. **12**, 043037 (2010).

13. R. Betti, W. Theobald, C. D. Zhou, K. S. Anderson, P. W. McKenty, S. Skupsky, D. Shvarts, V. N. Goncharov, J. A. Delettrez, P. B. Radha *et al.*, J. Phys.: Conf. Ser. **112**, 022024 (2008).

14. S. Gus'kov, X. Ribeyre, M. Touati, J.-L. Feugeas, Ph. Nicolaï, and V. Tikhonchuk, Phys. Rev. Lett. **109**, 255004 (2012).

15. X. Ribeyre, S. Gus'kov, J.-L. Feugeas, Ph. Nicolaï, and V. T. Tikhonchuk, Phys. Plasmas **20**, 062705 (2013).

16. A. R. Piriz, G. Rodriguez Prieto, N. A. Tahir, Y. Zhang, S. D. Liu, and Y. T. Zhao, Phys. Plasmas **19**, 122705 (2012).

17. W. Theobald, R. Nora, W. Seka, M. Lafon, K. S. Anderson, M. Hohenberger, F. J. Marshall, D. T. Michel, A. A. Solodov, C. Stoeckl *et al.*, Phys. Plasmas **22**, 056310 (2015).

18. R. Nora and R. Betti, Phys. Plasmas **18**, 082710 (2011).

19. J. Delettrez, R. Epstein, M. C. Richardson, P. A. Jaanimagi, and B. L. Henke, Phys. Rev. A **36**, 3926 (1987).

20. K. S. Anderson, R. Betti, P. W. McKenty, T. J. B. Collins, M. Hohenberger, W. Theobald, R. S. Craxton, J. A. Delettrez, M. Lafon, J. A. Marozas *et al.*, Phys. Plasmas **20**, 056312 (2013).

21. V. N. Goncharov, T. C. Sangster, T. R. Boehly, S. X. Hu, I. V. Igumenshchev, F. J. Marshall, R. L. McCrory, D. D. Meyerhofer, P. B. Radha, W. Seka *et al.*, Phys. Rev. Lett. **104**, 165001 (2010).

22. J. D. Lindl, Phys. Plasmas **2**, 3933 (1995).

23. K. Kanaya and S. Okayama J. Phys. D: Appl. Phys. **5**, 43 (1972).

24. E. Llor Aisa, X. Ribeyre, S. Gus'kov, Ph. Nicolaï, and V. T. Tikhonchuk, Phys. Plasmas **22**, 102704 (2015).

25. R. Fonseca, L. Silva, F. Tsung, V. Decyk, W. Lu, C. Ren, W. Mori, S. Deng, S. Lee, T. Katsouleas et al, Lect. Notes Comput. Sci. **2331**, 342 (2002).

26. R. Yan, J. Li, and C. Ren, Phys. Plasmas **21**, 062705 (2014).

27. O. Klimo, S Weber, V. T. Tikhonchuk, and J. Limpouch, Plasma Phys. Control. Fusion **52**, 055013 (2010).

28. X. Ribeyre, G. Schurtz, M. Lafon, S. Galera, and S. Weber, Plasma Phys. Control. Fusion **51**, 015013 (2009).

29. A. Bose, K. M. Woo, R. Nora, and R. Betti, Phys. Plasmas **22**, 072702 (2015).

30. K. M. Woo, R. Betti, A. Bose, R. Epstein, J. A. Delettrez, K. S. Anderson, R. Yan, P.-Y. Chang, D. Jonathan, and M. Charissis, "Three-Dimensional Simulations of the Deceleration Phase of Inertial Fusion Implosions," presented at the 57th Annual Meeting of the APS Division of Plasma Physics, Savannah, GA, 16–20 November 2015.

31. A. Bose, K. M. Woo, R. Betti, E. M. Campbell, D. Mangino, A. R. Christopherson, R. L. McCrory, R. Nora, S. P. Regan, V. N. Goncharov et al, Phys. Rev. E **94**, 011201(R) (2016).

32. A. A. Solodov and R. Betti, Phys. Plasmas **15**, 042707 (2008).

33. H. W. Lewis, Phys. Rev. **78**, 526 (1950).

34. W. L. Shang, R. Betti, S. X. Hu, K. M. Woo, A. Bose, and A. R. Christopherson, "Two-Dimensional Simulations of Electron Shock Ignition at the Megajoule Scale," presented at the 58th Annual Meeting of the APS Division of Plasma Physics, San Jose, CA, 31 October–4 November 2016.

35. A. Colaïtis, X. Ribeyre, E. Le Bel, G. Duchateau, Ph. Nicolaï, and V. Tikhonchuk, Phys. Plasmas **23**, 072703 (2016).

36. Ph. Nicolaï, J.-L. Feugeas, M. Touati, X. Ribeyre, S. Gus'kov, and V. Tikhonchuk, Phys. Rev. E **89**, 033107 (2014).

37. P. W. McKenty, V. N. Goncharov, R. P. J. Town, S. Skupsky, R. Betti, and R. L. McCrory, Phys. Plasmas **8**, 2315 (2001).

38. S. X. Hu, V. N. Goncharov, P. B. Radha, J. A. Marozas, S. Skupsky, T. R. Boehly, T. C. Sangster, D. D. Meyerhofer, and R. L. McCrory, Phys. Plasmas **17**, 102706 (2010).

39. P. Y. Chang, R. Betti, B. K. Spears, K. S. Anderson, J. Edwards, M. Fatenejad, J. D. Lindl, R. L. McCrory, R. Nora, and D. Shvarts, Phys. Rev. Lett. **104**, 135002 (2010).

40. R. Betti, A. R. Christopherson, B. K. Spears, R. Nora, A. Bose, J. Howard, K. M. Woo, M. J. Edwards, and J. Sanz, Phys. Rev. Lett. **114**, 255003 (2015).

Figure captions

FIG. 1. (color online). Sketch of the electron shock ignition scheme (a) and planar model cited from Ref. [18] (b). In Ref. [18], the initial hot spot and shell density are uniform, and the isobaric initial condition is used. Here the initial conditions are taken from *LILAC* simulations.

FIG. 2. (color online). (a)Target and (b) laser pulse with (solid line) and without (dashed line) the shock power spike.

FIG. 3. (color online). (a)

(a) Time-dependent laser-to-hot-e conversion efficiencies from PIC simulations. The time-integrated laser-to-hot-e conversion efficiency above 50 keV is $\eta_{50} \sim 25\%$, and above 25 keV is $\eta_{25} \sim 31\%$. (b) The hot-spot pressure ratio $R = P_{\text{hot-e}} / P_{laser}$ versus the launching time. $P_{\text{hot-e}}$ and P_{laser} are the hot-spot pressures at stagnation driven by the hot-e's and laser.

FIG. 4. (color online). (a) Density (dotted line) and pressures with hot-e's (solid line), and without hot-e's (dashed line). The launching time is 10.3 ns with a hot-e energy of 25 kJ. (b) Gain versus launching time for a hot-e pulse with various energies.

FIG. 5. (color online). (a) Energy gain versus $\text{YOC}_{\text{no}\alpha}$ at 10.3 ns and 10.5 ns with different initial roughness conditions. (b) Density plot at the peak neutron rate with α-

heating and gain ~ 4 at 10.3 ns. (c) Corresponding density plot to Fig. 4(b) without α-heating. The hot-e energy is 25 kJ.

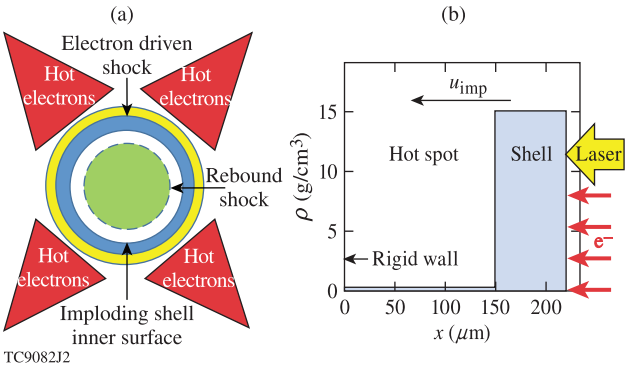

Figure 1 LA15672 06OCT2017

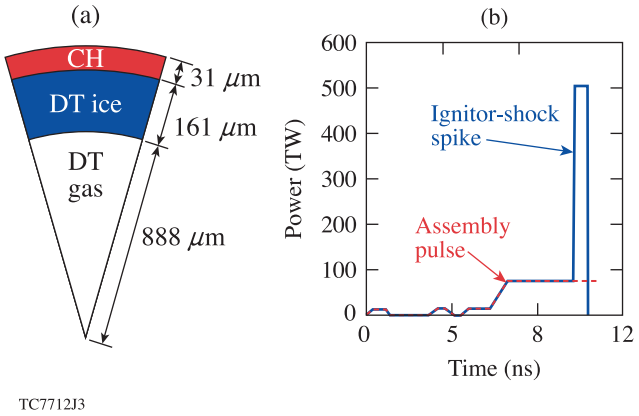

Figure 2 LA15672 06OCT2017

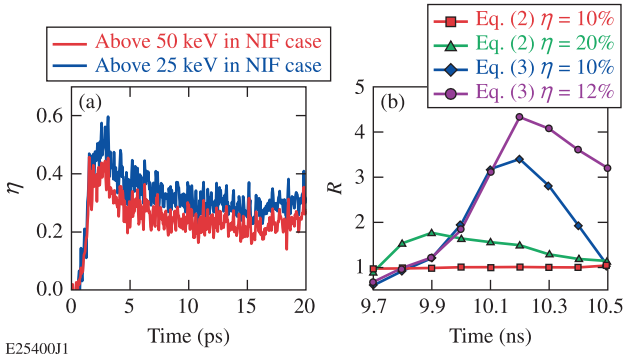

Figure 3 LA15672 06OCT2017

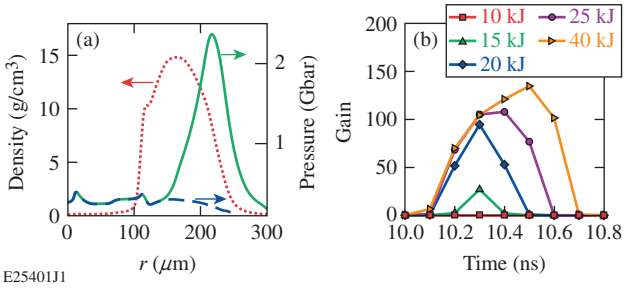

Figure 4 LA15672 06OCT2017

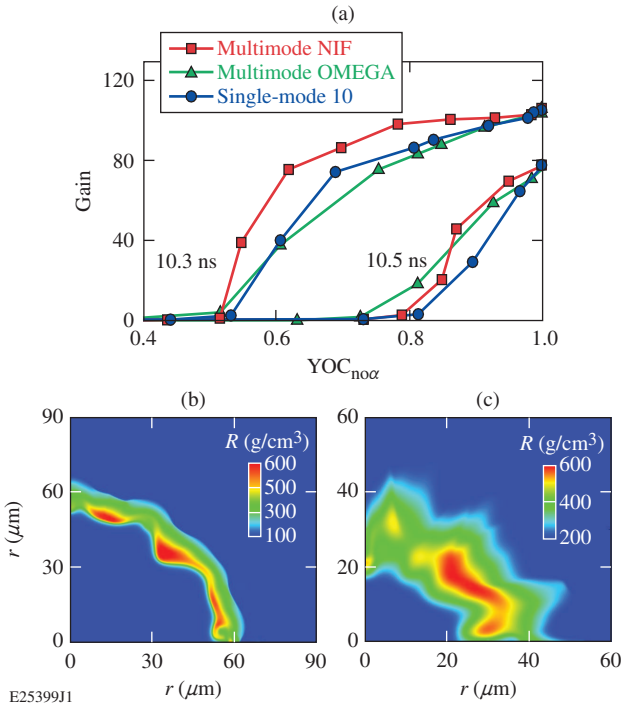

Figure 5 LA15672 06OCT2017